Motion-Compensated Cone Beam CT Using a Conjugate Gradient Least Squares Algorithm and EIT Imaging Motion Data

T Pengpen, M Soleimani*

Engineering Tomography Laboratory (ETL), Department of Electronic and Electrical Engineering, University of Bath, Bath UK.

Corresponding author's email: m.soleimani@bath.ac.uk

Abstract: Cone Beam Computed Tomography (CBCT) is an imaging modality that has been used in image-guided radiation therapy (IGRT). For applications such as lung radiation therapy, CBCT images are greatly affected by the motion artefacts. This is mainly due to low temporal resolution of CBCT. Recently, a dual modality of Electrical Impedance Tomography (EIT) and CBCT has been proposed, in which the high temporal resolution EIT imaging system provides motion data to a motion compensated algebraic reconstruction technique (ART) based CBCT reconstruction software. High computational time associated with ART and indeed other variations of ART make it less practical for real applications. This paper develops a motion-compensated conjugate gradient least squares (CGLS) algorithm for CBCT. A motion-compensated CGLS offers several advantages over ART based methods; including possibilities for: explicit regularisation, rapid convergence, and parallel computations. This paper for the first time demonstrates motion compensated CBCT reconstruction using CGLS and reconstruction results are shown in limited data CBCT considering only a quarter of full data set. The proposed algorithm is tested using simulated motion data in generic motion compensated CBCT as well as measured EIT data in dual EIT-CBCT imaging.

Keywords: *Cone beam CT, dual modality imaging, electrical impedance tomography, CGLS*

1. Introduction

Cone beam CT (CBCT) is an imaging system combined into linear accelerator (Linac) for verifying the treatment area in radiation therapy. Due to slow rotating CBCT motion artefacts are often appears in CBCT images in applications such as lung imaging. The motion artefacts can result in target registration errors and radiation beam misalignment, which in turn can lead to over-radiation dose to normal tissue and inhomogeneous distribution of radiation dose to the tumor (Goitein, 2004, Bortfeld et al., 2002, Balter et al., 1996). In addition, reconstruction with limited data has also been studied in order to reduce the radiation dose to the patients (Andersen, 1989, Chlewicki et al., 2001, Qiu et al., 2010). Motion will further degrade the limited data imaging.

In the last decade motion-compensated CBCT, for removing motion blur artefacts in CBCT scans, has attracted the interest of many research groups (Rit et al., 2009b, Shirato et al., 2000, Dietrich et al., 2006, Isola et al., 2008, Sonke et al., 2005, Purdie et al., 2006). Many reconstruction methods have been proposed for compensating the motion. Iterative algorithms e.g. the Algebraic Reconstruction Technique (ART), Simultaneous Algebraic Reconstruction Technique (SART) and Ordered-Subset SART (OS-SART) are the methods of choice (Gordon et al., 1970, Ge and Ming, 2004, Jiang and Wang, 2003, Raparia et al., 1997). Furthermore, motion compensation has been combined with ART and SART (Rit et al., 2009a, Pengpan et al., 2011).

Conjugate Gradient Least Squares (CGLS) is an attractive iterative reconstruction algorithms, which has been applied to CBCT image reconstruction by Jia X, et al (Jia et al., 2011). The CGLS has advantage over ART and SART, in terms of faster convergence rate and possibility of parallel computation. In addition, the CGLS provides possibility of including regularisation term, which is useful for limited data. While the Feldkamp, Davis and Kress (FDK) reconstruction, is one of the most commonly used in many volumetric CT, imaging based on filtered-back projection (FBP), showed inappropriate method for insufficient projection data (SOIMU et al., 2003) and less

accurate reconstruction in comparison with iterative method reconstruction (SART), in particular with limited projection data (Chlewicki et al., 2001). CGLS has not been developed in motion compensated CBCT based on our best knowledge.

To our knowledge, the application of motion compensation to CGLS algorithm has not been reported. Therefore, it is proposed to apply fast image reconstruction CGLS with limited data, to remove motion blur artefacts on CBCT images and reduce the reconstruction time.

The ART based motion compensated algorithm has been tested in a previously proposed dual modality electrical impedance tomography (EIT), CBCT setting for potential lung imaging application (Pengpan et al., 2011). EIT is an imaging system recently found momentum in area of lung imaging. EIT can provide a 3D image of electrical conductivity distribution by measuring current and voltages at the boundary electrodes. EIT has low spatial resolution, but its high temporal resolution makes it as a very good candidate to provide motion information to CBCT. EIT based motion data is real time and instant observation based and so can be more reliable than an estimated model based motion data currently used in 4D CBCT. This paper presents simulation and phantom experimental studies.

Fig *1* shows a more complete idea of how the proposed scheme can be considered in future clinical studies. In this general plan, a patient specific model can be developed using high quality diagnostic CT images for patient specific modelling EIT imaging. The combined EIT-CBCT imaging will be used just before radiation session for treatment planning. In addition, one may be able use EIT imaging during radiation therapy for adaptive real time treatment, which is outside of the scope of the current paper. The area shown in Fig 1 (dashed-line ellipse) is the subject of this work.

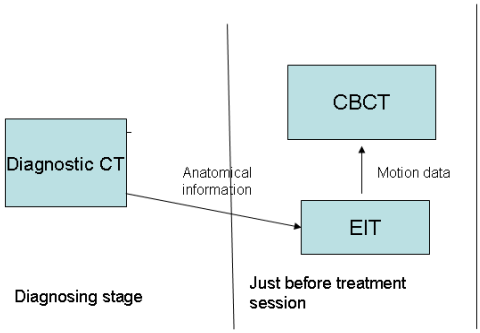

***Fig** 1 Schematic diagram of proposed combined imaging system*

The main aim of this work is to investigate the effectiveness of the motion-compensated CBCT using proposed CGLS algorithm together with the EIT system for limited projection data reconstruction as shown in Fig 1. In this set up, the EIT will provide information about the movement of the organ(s). The motion data will then be used to enhance the CBCT images. In this paper the motion-compensated CGLS was developed and tested for the improvement of CBCT image reconstruction using one-fourth projection data. The motion-compensated CGLS was applied to the dual modality EIT-CBCT (Pengpan et al., 2011) by utilising the motion estimated from EIT images. A better performance of motion compensated CBCT can be seen here due to the possibility of regularisation terms that can be included in CGLS scheme.

2. Image reconstruction methods

This section presents the image reconstruction methods used for CBCT and EIT. Imaging results are displayed as reconstructed images and one-dimensional plots and are analysed in terms of the Root Mean Square Error (RMSE) of reconstructed images compared with the true image as follows:

$$RMSE = \sqrt{\frac{\sum_{i=1}^{N}(x_i - g_i)^2}{N}}, \tag{1}$$

where N is the number of voxles, x_i and g_i are the reconstructed and true value in the ith voxel, respectively.

2.1 EIT image reconstruction

An EIT is an imaging technique of impedance distribution within electrically conductive objects from surface electrical measurements. The main advantage of EIT is its high temporal resolution. EIT imaging was proposed to use as motion monitoring system in this study. To generate the EIT images, forward problem needs to be solved, which can be performed using a finite element method. The forward problem is a problem of estimating the measured EIT data with given conductivity distribution. The image reconstruction problem is an inverse problem and so to solve the inverse problem the forward modeling is needed. Under low-frequency assumptions, the full Maxwell's equations can be simplified to the complex-valued Poisson equation:

$$\nabla \cdot (\sigma \nabla \mathbf{u}) = 0 \tag{2}$$

where **u** is the complex-valued electric potential and σ is the conductivity of the medium. Appropriate boundary conditions (complete electrode model) are needed to enable a representative model for the EIT measurement process. In this work the complete electrode model is adapted, which took into account both the shunting effect of the electrodes and the contact impedance between the electrodes and tissue. Using this boundary condition the EIT model includes

$$u + z_l \sigma \frac{\partial u}{\partial n} = U_l, \ r_x \in e_l, l = 1,2,\ldots,L \tag{3}$$

$$\int_{e_l} \sigma \frac{\partial u}{\partial n} dS = I_l, \ r_x \in e_l, l = 1,2,\ldots,L \tag{4}$$

$$\sigma \frac{\partial u}{\partial n} = 0, \ r_x \in \partial\Omega / \cup_l^L e_l \tag{5}$$

where z_l is the effective contact impedance between the l^{th} electrode and the tissue, n is the outward normal to the surface electrodes, U is the complex-valued voltage, I is the complex-valued current and e_l denotes the electrode l. Here, $r_x \in \partial\Omega / \cup_l^L e_l$ indicates a point on the boundary not under the electrodes. Difference imaging mode with a Tikhonov type algorithm has been used for the image reconstruction:

$$\Delta\sigma = (\mathbf{J}^T \mathbf{J} + \delta\mathbf{R})^{-1} \mathbf{J}^T \Delta\mathbf{V} \qquad (6)$$

where **R** is the regularization matrix (identity matrix here), **J** is the Jacobian matrix, $\mathbf{\Delta V}$ is the measurement vector, δ is the regularization parameter, which has been selected empirically with test samples in experimental data.

Our 16 electrode EIT system in a LabVIEW environment based on National Instruments (NI) cards was used in this study (Pengpan et al., 2011). Fig 2 shows the imaging capability of the EIT system used in this study, $\delta = 0.001$ is a suitable choice for the regularization parameter here. Fig 2 (b) shows the EIT reconstructed image of four bottles in a tank phantom (fig 2 (a)). Adjacent current pattern with the electric current of 5 mA in a single frequency of 10 kHz was used. The same EIT system, algorithm and EIT phantom was used for experimental study for dual modality EIT-CBCT presented in section 4.

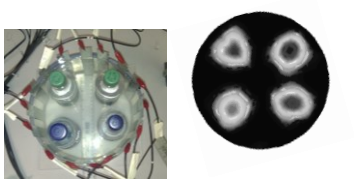

(a) (b)

Fig 2 *An example of EIT image reconstruction for four inclusions*

2.2 Motion-compensated CGLS Algorithm for CBCT

CGLS is an iterative method well suited for large sparse least squares problem of **Ax=b,** in CBCT reconstruction **x** is the image values for $\mathbf{x} \in \Re^N$ and **b** is observed data

for $\mathbf{b} \in \Re^M$. The weighting ($\mathbf{A} \in \Re^{M \times N}$) is created using a forward projection programme. Matrix **A** is a combination of the sub-matrix for each projection. The length of intersection of m^{th} ray with n^{th} cell is $\mathbf{A}_{mn}$. In the case where matrix **A** is positive-definite, then the matrix $\mathbf{A}^T\mathbf{A}$ is positive-definite for any matrix **A**. The iterative method is terminated at most i steps for $k = 0, 1, 2, \ldots, i$. The residual ($\mathbf{r}^k$) at each step is computed by (Hestenes and Stiefel, 1952, Bjorck, 1996, Hansen, 1998)

$$\mathbf{r}^k = \mathbf{b} - \mathbf{A}\mathbf{x}^k \tag{7}$$

Starting with initial approximation ($\mathbf{x}^0$), then, $\mathbf{r}^0 = \mathbf{b} - \mathbf{A}\mathbf{x}^0$, $\mathbf{p}^0 = \mathbf{A}^T\mathbf{r}^0$, where **p** is mutually conjugate direction.

and

$$\alpha^k = \frac{\left\|\mathbf{A}^T\mathbf{r}^{k+1}\right\|^2}{\left\|\mathbf{A}\mathbf{p}^k\right\|^2} \tag{8}$$

$$\mathbf{x}^{(k+1)} = \mathbf{x}^k + \alpha^k\mathbf{p}^k \tag{9}$$

$$\mathbf{r}^{(k+1)} = \mathbf{r}^k - \alpha^k\mathbf{A}\mathbf{p}^k \tag{10}$$

$$\beta^k = \frac{\left\|\mathbf{A}^T\mathbf{r}^{k+1}\right\|^2}{\left\|\mathbf{A}^T\mathbf{r}^k\right\|^2} \tag{11}$$

$$\mathbf{p}^{k+1} = \mathbf{A}^T\mathbf{r}^{k+1} + \beta^k\mathbf{p}^k \tag{12}$$

Normally, an initial approximation is $\mathbf{x}^0 = 0$, then $\mathbf{r}^0 = \mathbf{b}$ and $\mathbf{p}^0 = \mathbf{A}^T\mathbf{b}$. In case the residual **r** is zero, it implies that the problem is solved. Otherwise, if the residual r is non-zero, the desired solution for $\mathbf{r}^k$ to be minimised, which can be monitored by the L2 norm of the $\mathbf{r}^k$ for each iteration. This can be achieved by updating the residual **r** into the problem iteratively.

For motion-compensated CGLS, a motion compensation technique based on our previous report (Pengpan et al., 2011) was used. The weight matrix **A** which is partitioned into sub-matrices to be shifted its column appropriately applied according to a motion model

to each measured projection. This technique implements the motion compensation into a matrix **A** rather than image side **x**. The weight matrix $\mathbf{A} \in \Re^{M \times N}$ was partitioned by row into sub-matrices that correspond to each unique projection. The motion compensation was then applied separately for each sub-matrix, by shifting the columns within each sub-matrix according to the motion model for the relevant projection. For this reason, the motion must be estimated for each and every projection.

To evaluate the motion-compensated CGLS, two types of motions: "correct motions", assuming the motion was exactly known and "approximated motion" are considered, assuming that the motion was known but with some error. In "correct motion compensation", matrix **A** was compensated by applying the same amount of motion as applied to the phantom for each projection. Considering limited spatial resolution in EIT imaging the "approximated motion compensation" is closer to EIT motion data. This has been investigated in previous study (Pengpan et al., 2011), where images with 10% error in motion data could have sufficiently compensates for motion artefacts in CBCT images. For "approximated motion compensation", matrix **A** was shifted by the motion signals extracted from EIT images for the relative projection.

Moreover, regularised CGLS was also studied here for limited data problems. Limited data generally require regularisation terms for the image reconstruction. Standard Tikhonov is one of the commonly used methods for regularisation. It was used in this study to create a regularised CGLS as follows:

$$\begin{bmatrix} \mathbf{A} \\ \lambda \mathbf{R} \end{bmatrix} \mathbf{x} = \begin{bmatrix} \mathbf{b} \\ 0 \end{bmatrix} \tag{13}$$

where λ is the regularization parameter, **R** is the regularization matrix, which is the identity matrix in this case.

2.2.1 CGLS reconstruction of consistent and inconsistent phantom

These are the results of CGLS reconstruction of CBCT for consistent phantom and inconsistent phantom. Fig 3 (a) shows image error plot between reconstructed images and the true image (fig 3 (b)) for both cases. The behaviours of consistency and inconsistency were similar to each other for the first few iterations. After the 12th iteration, the reconstruction of the consistent phantom remained steady, but, for the inconsistent phantom, the reconstruction after the 8th iteration diverged. Reconstructed images at the 1st and the 12th iteration of the consistent phantom are shown in fig 3 (c) and fig 3 (d); and reconstructed image at the 1st and the 12th iteration of inconsistent phantom are shown in fig 3 (e) and fig 3 (f), respectively. These results clearly showed the sharper images for consistent phantom.

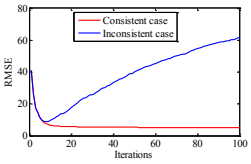

(a)

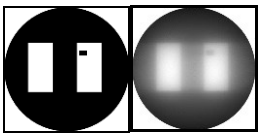

(b) (c)

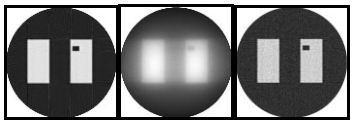

(d) (e) (f)

Fig 3 *(a) RMSE of CGLS reconstruction algorithm for consistent case and in consistent case; reconstructed images at (b) the true image, (c) the 1st iteration of consistent phantom, (d) the 12th iteration of consistent phantom, (e) the 1st iteration of inconsistent phantom and (f) the 12th iteration of inconsistent phantom.*

2.2.2 Regularised CGLS for inconsistent phantom

Due to the divergence after a few iteration of the inconsistent phantom reconstruction, regularised CGLS was introduced in this study. Variation of regularisation parameter (λ) was also investigated. Fig 4 (a) shows RMSE of no regularised CGLS and regularised CGLS with different values of the λ. The reconstructed images, after the 12th iterations, are shown in fig 4 (b) to (e). The RMSE plot shows that the appropriate λ value could be reduce divergence effects of the CGLS reconstruction for the inconsistent case. In this study, λ =10 gave the best convergence compared to no regularisation and regularisation for λ ={1, 100}. In conclusion, the regularisation with optimal regularisation parameter has a feasibility to keep the convergence of CGLS reconstruction for inconsistent case steadily after the 12th iteration. However, in this study the 12th iteration was chosen for the motion-compensated CGLS in order to keep the computational time minimal.

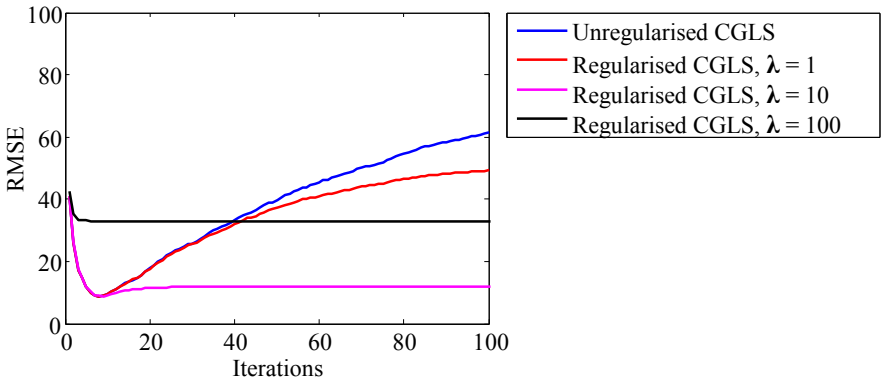

(a)

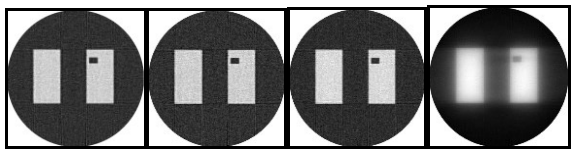

(b) (c) (d) (e)

Fig 4 *(a) RMSE comparing between un-regularised CGLS, regularised CGLS with λ ∈ {1, 10, 100}; reconstructed images of (b) un-regularised CGLS, (c) regularised CGLS with λ =1, (d) regularised CGLS with λ =10 and (e) regularised CGLS with λ =100.*

3. Motion compensated CBCT: simulated motion data

3.1 Simulated motion data

A simulated phantom was created for investigating motion-compensated CGLS image reconstruction using EIT motion signals. To test CGLS algorithm for the CBCT imaging, a consistent phantom was first reconstructed. However, the most clinical cases were inconsistency, the image reconstruction of inconsistent cases was also studied by corrupting the right hand side of the **Ax=b** with errors, so-called "inconsistency". The inconsistent cases were created by adding random Gaussian noise at 5% of the standard deviation for each projection data at each relative projection.

For testing the motion-compensated CGLS, a moving phantom was created by shifting the simulated phantom with 20 mm peak-to-peak amplitude of sinusoidal signal (fig 2) in

the up/down direction. Motion-compensated CGLS for the phantom when motion with additive motion error applied was subsequently evaluated. Three types of motion error (amplitude error, Gaussian error, and phase error) with different percentages of error were added into the original sinusoidal signal (fig 5). For amplitude error, 5%, 10%, 15% and 20% of the 20 mm peak-to-peak amplitude of the original sinusoidal signal was applied. Next, motion signals with additive Gaussian noises were created by adding Gaussian noises with standard deviation set to 5%, 10%, 15% and 20% of the 20 mm peak-to-peak amplitude of the original motion signal. Finally, phase errors were generated by using 2% to 20% with 2% interval of a complete cycle of the original signal. These motion signals with motion error were used to shift the phantom when collecting projection data.

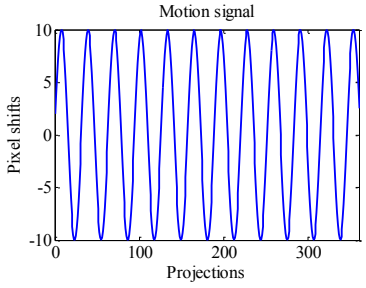

Fig 5 *A 20 mm peak-to-peak amplitude of sinusoidal signal.*

3.2 Motion-compensated CGLS

Motion-compensated CGLS algorithm (as described in Methods section) was tested in this part of the study. The RMSE of no motion applied, sinusoidal motion applied, and correct motion compensation when motion applied are shown in fig 6 (a). The plot of the correct motion compensation shows similarity behaviour as no motion applied. When the motion applied into data acquisition process, the image reconstruction shows motion blur artefacts can be easily seen in fig 6 (c). The results here suggested that the motion-compensated CGLS can be used to reduce the motion blur artefacts in CBCT image reconstruction.

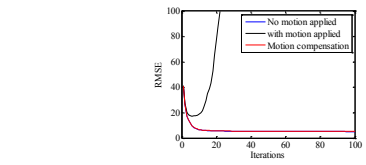

(a)

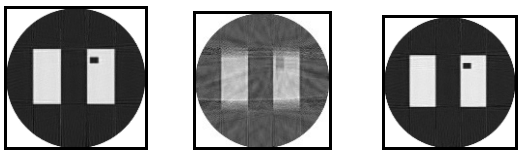

(b) (c) (d)

Fig 6 *(a) RMSE of reconstructed images when no motion applied, with motion applied and motion compensation applied; reconstructed image of (b) no motion applied, (c) motion applied, and (d) motion compensation applied.*

3.3 Motion-compensated CGLS when motion error applied

This was the study of 20 mm peak-to-peak amplitude of sinusoidal motion signal, corrupted by three types of motion error: amplitude error, Gaussian error, and phase error. Fig 7 (a) to (c) show RMSE of reconstructed images when motion error applied and motion-compensated CGLS used, and fig 7 (d) to (g) show the motion-compensated images after the 12^{th} iteration of no motion error applied and motion error applied for 20% of motion. The RMSE plots show that an increase in percentages of the motion error results in an increase in RMSE for all types of error. Phase shifting was the most effects to the motion-compensated CGLS when compared with amplitude error and Gaussian error. This can be clearly seen in the reconstructed images shown in fig 7 (d) to (g). The reconstructed image of phase error added (fig 7 (g)) shows higher blurring artefacts at the same level of motion error.

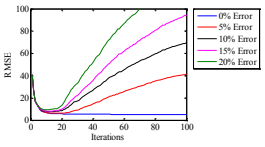

(a)

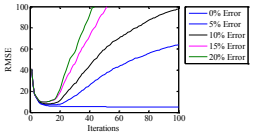

(b)

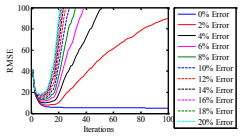

(c)

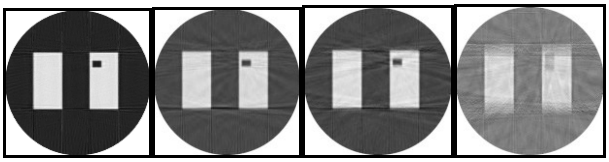

(d) (e) (f) (g)

Fig 7 *RMSE of motion compensation when different percentages of (a) amplitude error applied (b) Gaussian noise applied, and (c) phase error applied; reconstructed images of (d) 0% motion error, (e) 20% of amplitude error, (f) 20% of Gaussian error, and (g) 20% of phase error.*

4. Motion compensated CBCT: EIT phantom data

The motion information is extracted from a sequence of EIT images using a simple motion detection technique. This technique is an image processing thresholding technique developed and used in (Pengpan et al., 2011, Terzija et al., 2010). The image processing thresholding technique is converting the grey scale EIT images to binary images using the average of maximum and minimum pixel values for each image. The centre of objects within a binary image is extracted, and, then, is tracked for a sequence of images. This result in the difference in positions of centroids between the sequence images and the first image so called the motion signal extracted from EIT images.

The motion-compensated CGLS, using motion signals extracted from EIT images, was tested with a 50 mm diameter cylindrical object. This object was moved in the up/down

direction for 20 mm peak-to-peak displacement and 60 mm peak-to-peak displacement and in the left/right direction for 40 mm peak-to-peak.

The results of the motion-compensated CGLS using EIT motion signals for the up/down movement, are shown in fig 4 for 20 mm displacement and fig 6 for 60 mm displacement. Fig 8 shows the results of the motion-compensated CGLS using EIT motion signals for the left/right direction with 40 mm movement.

For the 20 mm up/down displacement, reconstructed images after the 12^{th} iteration are shown in fig 8 (a) to (d), RMSE is shown in fig 8 (e), and 1D plot is shown in fig 8 (f). It can be seen that fig 8 (b) is corrupted by motion. When correct motion compensation technique (as described above) was applied into image reconstruction process, the resulted image is shown in fig 8 (c). Furthermore, fig 8 (d) shows a motion-compensated image using motion signal extracted from EIT images. RMSE shows the behaviours of no motion applied and correct motion compensation were very similar. On the other hand, the motion compensation using EIT motion signal has higher image error than the correct motion compensation; however lower image error than motion applied. 1D plot also supports the results of the reconstructed images and the RMSE plot.

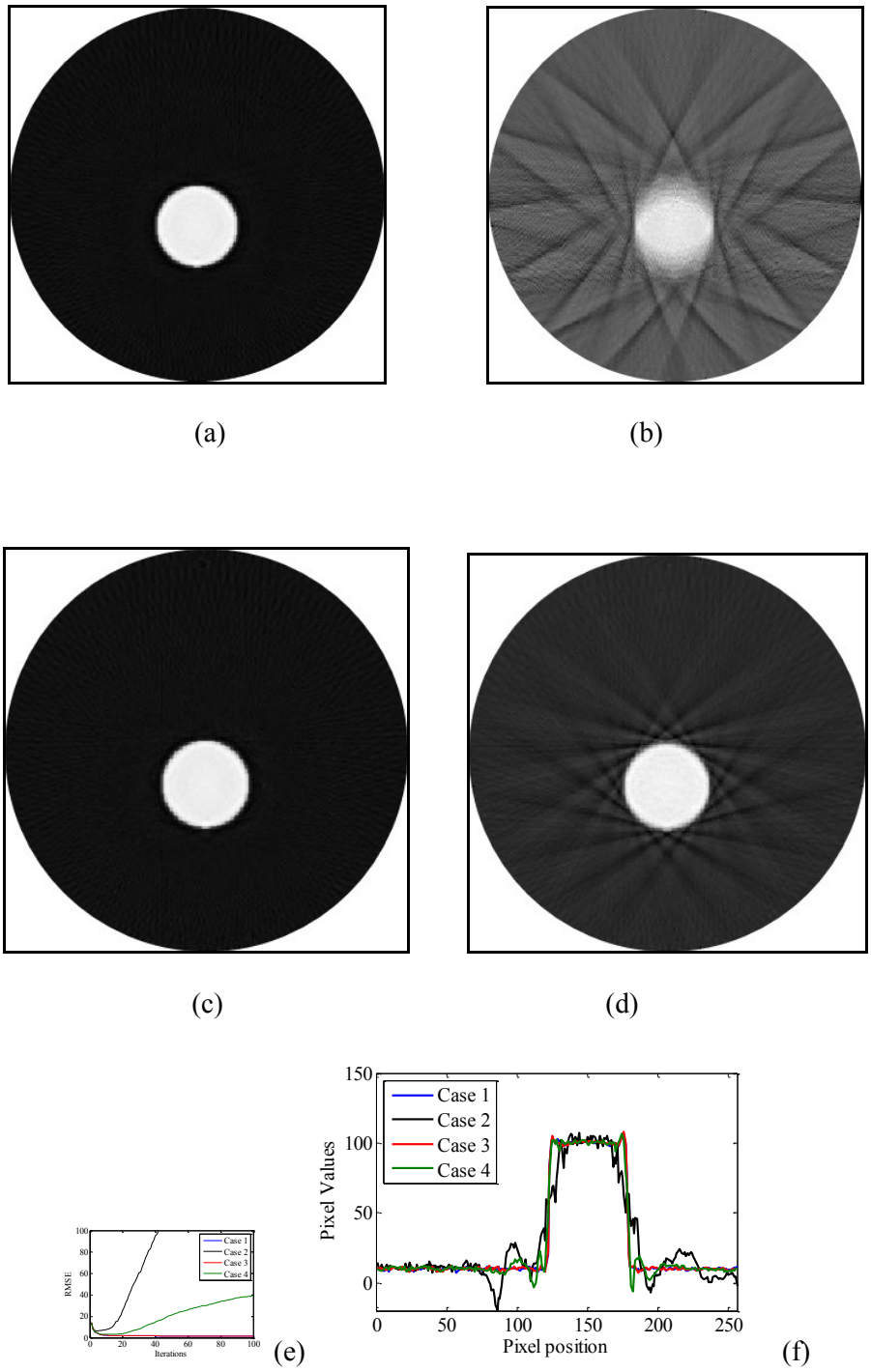

Fig 8 *CBCT Images with (a) no motion applied, (b) 20 mm peak-to-peak sinusoidal motion applied, (c) motion compensation applied using true motion signal and (d) motion compensation applied using motion signal extracted from EIT images; (e) RMSE of (a) to (d) compared with the true image (case 1: no motion applied; case 2: motion applied; case 3: motion compensation using actual signal; case 4: motion compensation using EIT signal) ; (f) 1D plots running through the centre of object (x=128) of (a) to (d) .*

The results of the 60 mm up/down displacement motion compensation are shown in fig 9. The reconstructed images of no motion applied, motion applied, correct motion compensation applied and motion compensation using EIT motion signal applied are given in fig 9 (a) to (d), respectively. Fig 9 (e) and (f) show RMSE and 1D plot of reconstructed images. It can be seen that the motion compensated image using EIT motion signal of 60 mm shows higher image noise than the motion compensated image using EIT motion signal of 20 mm.

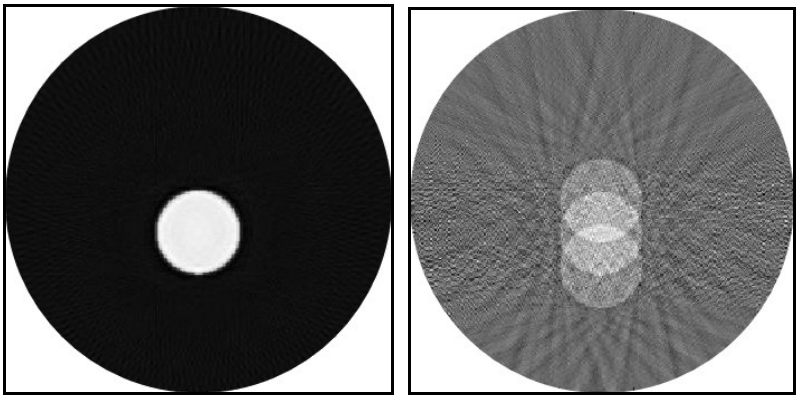

(a) (b)

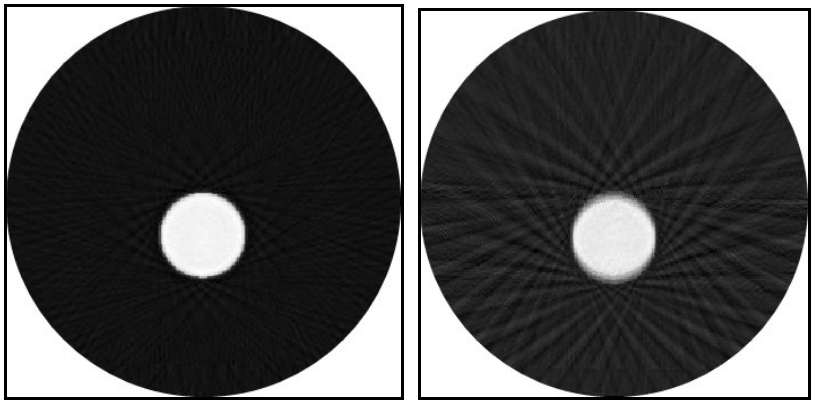

(c) (d)

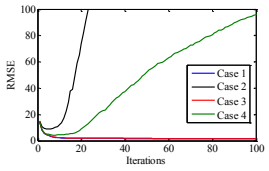

(e)

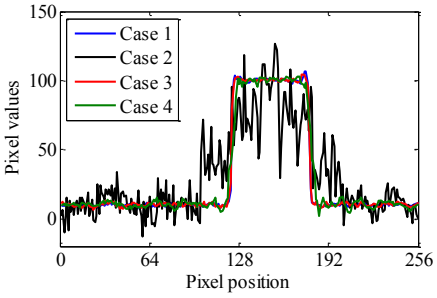

(f)

Fig 9 *CBCT Images with (a) no motion applied, (b) 60 mm peak-to-peak sinusoidal motion applied, (c) motion compensation applied using true motion signal and (d) motion compensation applied using motion signal extracted from EIT images; (e) RMSE of (a) to (d) compared with the true image (case 1: no motion applied; case 2: motion applied; case 3: motion compensation using actual signal; case 4: motion compensation using EIT signal); (f) 1D plots running through the centre of object (x=128) of (a) to (d) .*

The results of the motion compensation using EIT motion signal for 40 mm displacement in the left/right direction are shown in fig 10. Fig 10 (a) is the reconstructed image without motion applied. Blurring effect of the movement in CBCT reconstructed image can be noticeable in fig 10 (b). Fig 10 (c) and (d) are motion-compensated CGLS images after the 12^{th} iteration using correct motion signal and motion signal extracted from EIT images, respectively. RMSE plot shows the behaviour of motion compensation using correct motion signal is similar to the behaviour of no motion applied. In addition, the motion compensation using EIT motion signal can reduce the motion blur artefact on CGLS image reconstruction. One-dimensional plot running through the centre of object in fig 10 (a) to (d) is shown in fig 10 (f). The boundaries of the object, in motion-compensated images, are sharper than those of motion image.

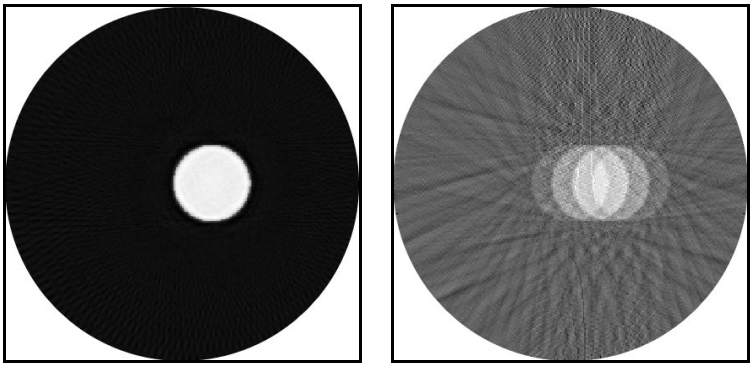

(a) (b)

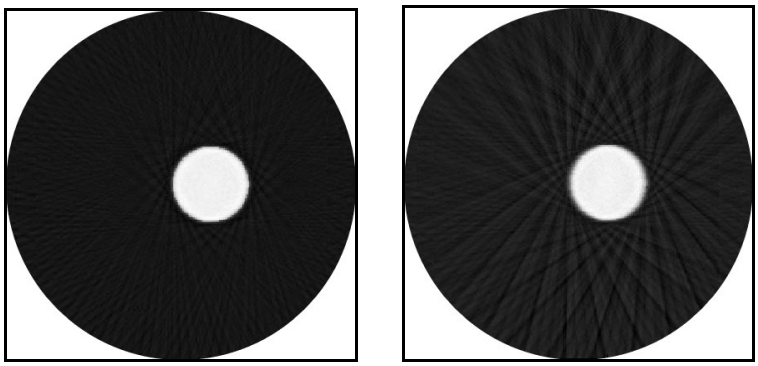

(c) (d)

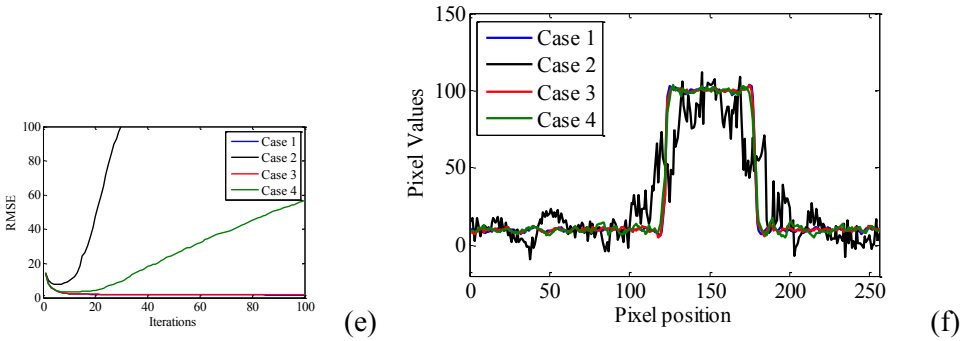

(e) (f)

Fig 10 *CBCT images with (a) no motion applied, (b) 40 mm peak-to-peak sinusoidal motion applied, (c) motion compensation applied using true motion signal and (d) motion compensation applied using motion signal extracted from EIT images; (e) RMSE of (a) to (d) compared with the true image (case 1: no motion applied; case 2: motion applied; case 3: motion compensation using actual signal; case 4: motion compensation using EIT signal); (f) 1D plots running through the centre of object (y=128) of (a) to (d) .*

Comparing among the motion-compensated images using EIT motion signal for 20, 40 and 60 mm displacements, motion artefacts for the 20 mm image is lower than those for the 40 mm and 60 mm images. These results suggested that motion-compensated CGLS by using EIT motion signal can reduce motion blur artefacts, especially for small amounts of motion. This implied that the efficiency of removing motion artefacts may depend on the accuracy of motion detection technique.

5. Conclusion

This paper presents a motion-compensated CBCT with limited data (one-fourth data) using CGLS reconstruction algorithm. CGLS is a superior iterative method compared to Kaczmarz's type methods (ART, SIRT, and SART), in terms of the speed of convergence, well suited for parallel computation, and possibility of including the regularisation and *a priori* knowledge in the image reconstruction process. The results suggested that the motion-compensated CGLS can improve image blur artefacts. Moreover, the motion-compensated CGLS was applied to our dual modality of EIT-CBCT, which uses the motion signal extracted from EIT images to compensate in CBCT image reconstruction. The results show that the motion signal extracted from EIT images can be used to compensate the motion artefact in CBCT image reconstruction by using proposed motion-compensated CGLS algorithm. Furthermore, the performance of motion compensation algorithm depends on the accuracy of motion signal. Further work will be required to implement this dual modality strategy in more meaningful clinical setting. Motion compensation can reduce blurring artefacts in CBCT scan, especially the movement of body organs e.g. heart, chest and abdomens.

References

ANDERSEN, A. H. 1989. Algebraic reconstruction in CT from limited views. *IEEE Trans Med Imaging,* 8**,** 50-55.

BALTER, J. M., TEN HAKEN, R. K., LAWRENCE, T. S., LAM, K. L. & ROBERTSON, J. M. 1996. Uncertainties in CT-based radiation therapy treatment planning associated with patient breathing. *International Journal of Radiation Oncology Biology Physics,* 36**,** 167-174.

BJORCK, A. 1996. *Numerical methods for least squares problems,* Philadelphia, Society for Industrial and Applied Mathematics.

BORTFELD, T., JOKIVARSI, K., GOITEIN, M., KUNG, J. & JIANG, S. B. 2002. Effects of intra-fraction motion on IMRT dose delivery: statistical analysis and simulation. *Physics in Medicine and Biology* 47**,** 2203–2220.

CHLEWICKI, W., BADEA, C. & PALLIKARAKIS, N. 2001. Cone based 3D reconstruction: A FDK-SART comparison for limited number of projections. *MEDICON,* June**,** 12-15.

DIETRICH, L., JETTER, S., TüCKING, T., NILL, S. & OELFKE, U. 2006. Linac-integrated 4D cone beam CT: first experimental results. *Physics in Medicine and Biology* 51**,** 2939-2952.

GE, W. & MING, J. 2004. Ordered-subset simultaneous algebraic reconstruction techniques (OS-SART). *Journal of X-ray Science and Technology,* 12**,** 169-177.

GOITEIN, M. 2004. Organ and tumor motion: an overview. *Seminars in Radiation Oncology,* 14**,** 2-9.

GORDON, R., BENDER, R. & HERMAN, G. T. 1970. Algebraic Reconstruction Techniques (ART) for three-dimensional electron microscopy and X-ray photography. *Journal of Theoretical Biology* 29**,** 471-481.

HANSEN, P. C. 1998. *Rank-deficient and discrete ill-posed problems: numerical aspects of liniear inversion,* Philadephia, Society for Industrial and Applied Mathematics.

HESTENES, M. & STIEFEL, E. 1952. Methods of conjugate gradients for solving linear systems. *Journal of Research of the National Bureau of Standards,* 49**,** 409-436.

ISOLA, A. A., ZIEGLER, A., KOEHLER, T., NIESSEN, W. J. & GRASS, M. 2008. Motion-compensated iterative cone-beam CT image reconstruction with adapted blobs as basis functions. *Physics in Medicine and Biology* 53**,** 6777-6797.

JIA, X., DONG, B., LOU, Y. & JIANG, S. B. 2011. GPU-based iterative cone-beam CT reconstruction using tight frame regularization. *Physics in Medicine and Biolology* 56**,** 3787-3807.

JIANG, M. & WANG, G. 2003. Convergence of the simultaneous algebraic reconstruction technique (SART). *IEEE Transactions on Image Processing,* 12**,** 957-61.

PENGPAN, T., SMITH, N. D., QIU, W., YAO, A., MITCHELL, C. N. & SOLEIMANI, M. 2011. A motion-compensated cone-beam CT using electrical impedance tomography imaging. *Physiological Measurement* 32**,** 19-34.

PURDIE, T. G., MOSELEY, D. J., BISSONNETTE, J.-P., SHARPE, M. B., FRANKS, K., BEZJAK, A. & JAFFRAY, D. A. 2006. Respiration correlated cone-beam computed tomography and 4DCT for evaluating target motion in Stereotactic Lung Radiation Therapy. *Acta Oncologica,* 45**,** 915-922.

QIU, W., TONG, J., MITCHELL, C., MARCHANT, T., SPENCER, P., C.J.MOORE & SOLEIMANI, M. 2010. New iterative cone beam CT reconstruction software: parameter optimisation and convergence study. *Computer Methods and Programs in Biomedicine* 100**,** 166-174.

RAPARIA, D., ALESSI, J. & KPONOU, A. Year. The Algebraic Reconstruction Technique (ART). *In:* Particle Accelerator Conference, 12-16 May 1997 1997 Vancouver, Canada IEEE, 2023-2025.

RIT, S., SARRUT, D. & DESBAT, L. 2009a. Comparison of analytic and algebraic methods for motion-compensated cone-beam CT reconstruction of the thorax. *IEEE Transactions on Medical Imaging,* 28**,** 1513-1525.

RIT, S., WOLTHAUS, J. W. H., VAN HERK, M. & SONKE, J.-J. 2009b. On-the-fly motion-compensated cone-beam CT using an a priori model of the respiratory motion. *Medical Physics,* 36**,** 2283-2296.

SHIRATO, H., SHIMIZU, S., KITAMURA, K., NISHIOKA, T., KAGEI, K., HASHIMOTO, S., AOYAMA, H., KUNIEDA, T., SHINOHARA, N., DOSAKA-AKITA, H. & MIYASAKA, K. 2000. Four-dimensional treatment planning and fluoroscopic real-time tumor tracking radiotherapy for moving tumor. *International Journal of Radiation Oncology Biology Physics* 48**,** 435-442.

SOIMU, D., BADEA, C. & PALLIKARAKIS, N. Year. Image Quality in Cone-Beam 3D reconstructions using Feldkamp algorithm: Acquisition Problems. *In:* the proceedings of the "MEDINF'2003" International Conference on Medical Informatics & Engineering, Craiova, Romania, October 9, 2003.

SONKE, J.-J., ZIJP, L., REMEIJER, P. & VAN HERK, M. 2005. Respiratory correlated cone beam CT. *Medical Physics,* 32**,** 1176-1186.

TERZIJA, N., PENGPAN, T., PEYTON, A. J., YIN, W. & SOLEIMANI, M. 2010. Extraction of motion information from electromagnetic induction tomography for flow imaging. *6th*

World Congress on Industrial Process Tomography. Beijing, China: Sage Publications, Inc.